Analysis of ^{13}C and ^{17}O Chemical Shift Tensors and an ELF View of Bonding in $Fe_2(CO)_9$ and $Rh_6(CO)_{16}$☆

Martin Kaupp

Institut für Theoretische Chemie, Universität Stuttgart,
Pfaffenwaldring 55, D-70569 Stuttgart, Germany

Max-Planck-Institut für Festkörperforschung,
Heisenbergstraße 1, D-70569 Stuttgart, Germany
Telefax: (internat.) +49(0)711/689-1562; E-mail: kaupp@vsibm1.mpi-stuttgart.mpg.de

Received December 27, 1995

Key Words: Density functional theory / Electron localization function / NMR chemical shift tensor / Transition-metal carbonyl clusters

Carbon and oxygen chemical shift tensors for bridging and terminal carbonyl ligands in $Fe_2(CO)_9$ and $Rh_6(CO)_{16}$ were calculated by sum-over-states density-functional perturbation theory (SOS-DFPT). Agreement with experimental ^{13}C shift tensors is excellent, and ^{17}O shift tensors are predicted. The reduced anisotropy values of the shift tensors for the bridging compared to terminal carbonyl ligands are due to large deshielding contributions to δ_{33} from non-bonding or bridge-bonding orbitals. Comparison to recent computational results for a series of unusual piano-stool and bent-sandwich group-4 complexes is made. The electronic structures of the clusters are discussed by using plots of electron localization functions (ELF). Bonding electrons within the Rh_6 cluster are mainly localized on the unbridged octahedral faces. This leads to a heterocubane-like arrangement of ELF maxima above all octahedral faces (four bridging CO ligands, four M–M 3-center-bonding maxima), in analogy to previous results for $B_6H_6^{2-}$.

The ^{13}C-NMR chemical shift tensors of terminal and of bridging carbonyl ligands in transition-metal clusters differ significantly. In particular, the bridging ligands exhibit reduced anisotropy of the shift tensor[1–3] and, for a given metal center, larger isotropic shifts[1–4]. This allows the distinction between bridging and terminal carbonyl positions by NMR spectroscopy through the isotropic shifts in solution, but even more clearly through the shift anisotropy values obtainable in suitable solid-state experiments.

An exception to this situation is given by the unusually large ^{13}C shifts of the *terminal* carbonyl ligands in a number of highly reduced piano-stool or bent-sandwich complexes of the group-4 metals (Ti, Zr, Hf)[5]. Using a novel density-functional theory approach[6–8], we could recently show by quantum-chemical calculations[9] that these remarkable ^{13}C shifts are accompanied by very low shift anisotropy values, which are more typical for bridging than for terminal ligands. Both the large isotropic shifts and the reduced anisotropy are due to deshielding contributions to the shift tensors from formally nonbonding, extended metal d orbitals of suitable spatial orientation. The same calculations predicted that the ^{17}O shifts of the carbonyl ligands are also unusually large, with low shift anisotropy[9].

In view of these surprising results for nominally terminal carbonyl ligands, a comparative examination of the shielding tensors for bridging carbonyl ligands in multinuclear clusters is of great interest. The combination[7,8] of ab initio effective-core potentials (ECPs) with sum-over-states density-functional perturbation-theory (SOS-DFPT)[6] used in our previous studies has turned out to be a powerful tool for the accurate calculation and interpretation of ligand chemical shifts in transition-metal complexes[7–11]. Due to its relatively low cost (compared to more traditional ab initio approaches to account for electron correlation), the ECP/SOS-DFPT method is also applicable to multinuclear clusters[11].

Here we examine the ^{13}C and ^{17}O chemical shift tensors in the two prototypical clusters $Fe_2(CO)_9$ and $Rh_6(CO)_{16}$. These compounds provide examples for doubly and triply bridging carbonyl ligands, respectively (and also for terminal ligands). Their carbon shift tensors have been studied in detail experimentally[1,2]. The presence of metal–metal bonding in the rhodium cluster but its apparent absence in the iron compound are interesting additional features. Among other things we want to address the following questions: (i) Is the reduced ^{13}C shift anisotropy of bridging carbonyl ligands also due to nonbonding metal d orbitals, as we found[9] for the abovementioned "unusual" terminal ligands? (ii) How different are oxygen shift tensors for bridging vs. terminal carbonyl ligands (no ^{17}O shift tensors for bridging carbonyl ligands have been measured up to now, but isotropic shifts appear to be very large[12])? We also examine the dependence of the shift tensors in $Fe_2(CO)_9$ on the bridging/semi-bridging character of the ligand.

The concise description of metal-metal vs. metal-ligand bonding in delocalized multinuclear transition-metal clusters is still a difficult task. We have plotted the electron

  0009–2940/96/0505–0527 $ 15.00+.25/0

localization function (ELF)[13] for the two title compounds. ELF provides very instructive local views of bonding in these clusters and also allows the visual comparison of the electronic characteristics for terminal and bridging ligands.

Computational Methods

The approximations involved in the sum-over-states density-functional perturbation theory (SOS/DFPT) approach have been discussed in detail in ref.[6]. The combination of SOS/DFPT with metal ECPs was first detailed in ref.[7], with subsequent applications in refs.[8–11]. The calculations were carried out with individual gauges for localized orbitals (IGLO)[14]. The IGLO procedure employed orbitals localized by the Foster/Boys scheme[15]. The C and O 1s orbitals were localized separately from the valence orbitals. The exchange-correlation functional of Perdew and Wang (1991)[16] was used. All SOS/DFPT calculations were carried out with a modified version of the deMon program[17].

The structural parameters for $Fe_2(CO)_9$ were taken from an X-ray diffraction study[18] and were idealized to D_{3h} symmetry (Figure 1a). Starting from this structure, slightly modified arrangements were created by changing the position of one of the bridging carbonyl ligands while keeping the rest of the molecule fixed (Figure 1b–d). Thus, structure A_1 (Figure 1b) is still relatively close to the experimental one (A_0). It corresponds closely to the arrangement of one semi-bridging carbonyl ligand in $Fe_3(CO)_{12}$[19]. The semi-bridging character is stronger in structure A_2 (cf. Figure 1c), comparable to a bridge in $Fe_3(CO)_{11}PPh_3$[20]. The bridge becomes very unsymmetrical in structure A_3 (Figure 1d), which corresponds to that of a semi-bridging ligand in $Fe_2(CO)_6PhC{\equiv}CPh$[21]. The structure of $Rh_6(CO)_{16}$ was also taken from an X-ray diffraction study[22] and idealized to T_d symmetry (Figure 2).

Quasirelativistic, energy-adjusted ECPs [keeping the $(n-1)$s and $(n-1)$p semi-core orbitals in the valence space] and (8s7p6d)/[6s5p3d] valence basis-sets were used for Fe[23] and Rh[24]. Three different strategies were followed with respect to the ligand basis sets. In one calculation on $Fe_2(CO)_9$ (at the experimental structure A_0), the IGLO-II all-electron basis[14] was used for all carbon and oxygen atoms. In comparative calculations for structures $A_0 - A_3$, only one distinct bridging CO ligand (the position of which was varied) was treated with this IGLO-II all-electron basis, whereas ECPs and (4s4p)/[2s2p] valence bases[25] were employed for all other ligands. We have previously shown for mononuclear carbonyl complexes that this "extended locally-dense basis approximation" yields satisfactory results and reduces the size of the basis set (and thus the computational cost) considerably[7]. In the present case, the mixed-basis approach reduces the number of basis functions from 492 to 252. Chesnut's locally-dense basis approach[26] in its original all-electron sense was used for $Rh_6(CO)_{16}$, that is IGLO-II basis sets were used on one bridging and on one terminal carbonyl ligand (for which the chemical shift tensors will be discussed), whereas somewhat more contracted, unpolarized valence double-ζ all-electron bases[27] were employed on the remaining ligands (the overall basis-set size

Figure 1. Structures used for $Fe_2(CO)_9$. a) Experimental structure (ref.[18]). b)–d) Modifications of one carbonyl bridge, see text

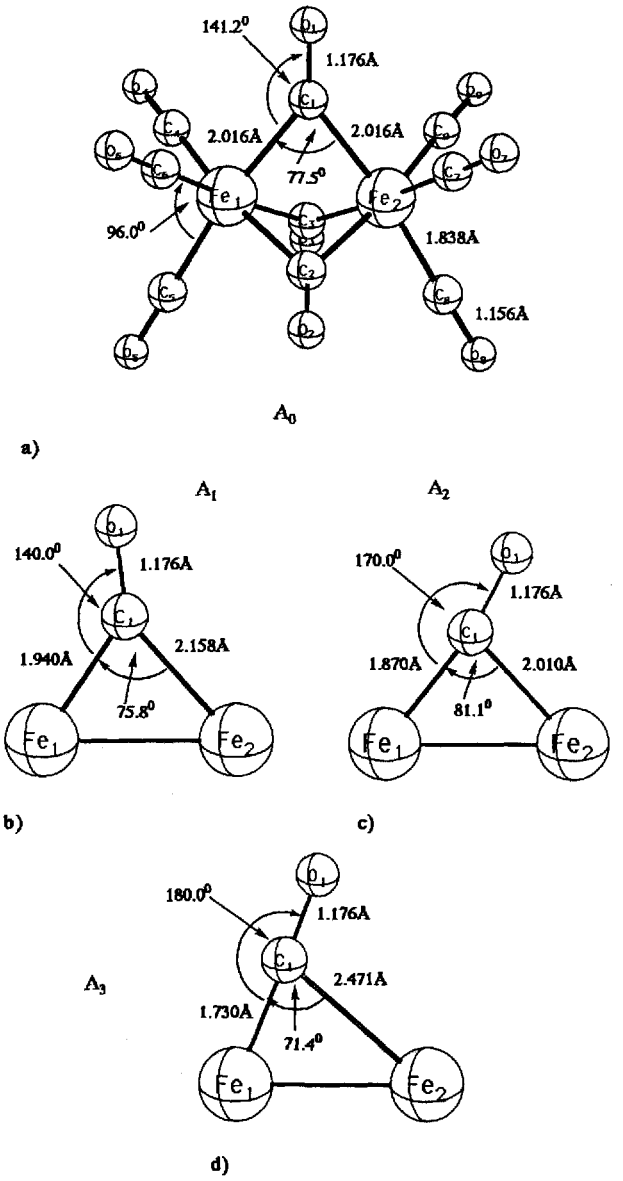

was 578 functions). Auxiliary basis sets for the fit of exchange-correlation potential and charge density were of the sizes 3,4 for the metals, 5,2 for carbon and oxygen with all-electron bases, and 3,2 for C and O with ECPs (n,m denotes n s functions and m spd shells[17]). In general, a "FINE" integration grid was used[6,17].

Shieldings for the reference compounds tetramethylsilane (TMS, for ^{13}C shifts) and H_2O^{vap} (for ^{17}O shifts) were calculated with the IGLO-II all-electron basis for all atoms. The absolute ^{13}C shielding of TMS at this level is 187.5 ppm, the ^{17}O shielding of the water molecule is 307.3 ppm. These values were used to convert computed absolute shieldings to chemical shifts.

The electron localization function (ELF)[13] was calculated for $Fe_2(CO)_9$ and $Rh_6(CO)_{16}$ for the experimental structures[18,22] by using ECPs and (4s4p1d)/[2s2p1d] valence bases[25] on all ligand atoms. The ELF isosurface plots

Figure 2. Ball-and-stick model of $Rh_6(CO)_{16}$ (structure from ref.[22]). Atomic labels are only given for the metals (white atoms), for the bridging carbon (black) and oxygen (shaded) centers

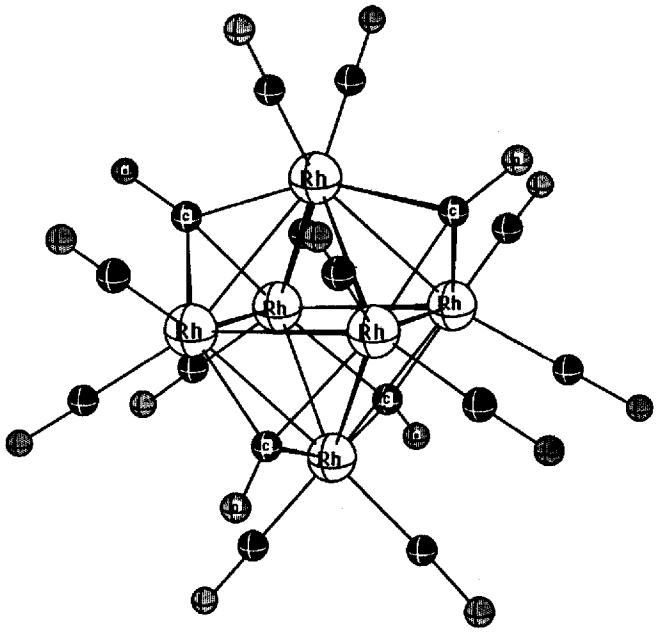

were based on Hartree-Fock results obtained with the TURBOMOLE program[28].

Results and Discussion

A. Shift Tensors in $Fe_2(CO)_9$

Table 1 lists the carbon and oxygen chemical shift tensors calculated with the full IGLO-II/ECP basis set and also experimental data for the carbon shift tensors. Agreement between most of the computed and experimental ^{13}C tensor elements is good. A somewhat larger deviation (shift 40 ppm too large) pertains to the computed δ_{33} of the bridging carbonyl carbon. As a result, the average shift δ_{av} is overestimated by 20 ppm, and the shift anisotropy $\Delta\delta$ is underestimated by 30 ppm.

The calculations distinguish well between bridging and terminal carbon atoms, that is they confirm the large deshielding contributions to δ_{33} ($\delta_{\|}$, the principal component of the shift tensor parallel to the C–O axis), the reduced anisotropy, and thus the increased isotropic shift δ_{av} for the bridging position. Our calculations for the oxygen shift tensors also show increased δ_{33} (as well as increased δ_{av} and reduced $\Delta\delta$) for the bridge oxygen atoms. Interestingly, δ_{11} and δ_{22} for the bridging oxygens are also somewhat larger than for the terminal ones, whereas the situation is rerversed for the ^{13}C shift tensor elements, particularly for δ_{22} (Table 1).

A breakdown of the shielding tensors into contributions from individual localized molecular orbitals (LMOs) as successfully employed for the analysis of mononuclear carbonyl complexes[9,10], is not straightforward for $Fe_2(CO)_9$. The LMOs obtained from the Foster-Boys procedure do not correspond to chemically reasonable Lewis structures, and they break the symmetry of the molecule. While this does not significantly affect the accuracy of the calculations, it does not allow an easy, local interpretation of the shielding tensors. Apart from well localized orbitals representing bonds to and within the terminal ligands, there also is a set of less well-defined orbitals corresponding to nonbonding metal d orbitals, to Fe–C–Fe bridging bonds, and to C≡O bonds of the bridging ligands. Contributions from these latter sets of LMOs account for the large δ_{33} of the carbon and oxygen nuclei of the bridging ligands. These "bridging" LMOs are also responsible for the deviations of the tensor from axial symmetry (i.e. $\delta_{11} \neq \delta_{22}$). A better visualization of bonding in $Fe_2(CO)_9$ than obtained from localized MOs is provided in subsection C by plots of electron localization functions (ELF)[13]. An LMO breakdown of the terminal ligand ^{13}C and ^{17}O shift tensors gives results very similar to those found previously for "typical" terminal carbonyl ligands, for example in $M(CO)_6$ (M = Cr, Mo, W)[4,10] or in $MCp(CO)_3$ (M = Mn, Tc, Re; Cp = η^5-C_5H_5)[9].

Table 1. Chemical shift tensors (ppm) for carbonyl groups in $Fe_2(CO)_9$[a]

		δ_{11}	δ_{22}	δ_{33}	δ_{av}	$\Delta\delta^b$
C_{bridge}	calc.	314.	260.	196.	257.	90.
	exp.	305.	249.	157.	237.	120.
C_{term}	calc.	350.	346.	-58.	213.	406.
	exp.	354.	339.	-77.	206.	423.
O_{bridge}	calc.	765.	696.	408.	623.	323.
O_{term}	calc.	616.	604.	-33.	396.	643.

[a] The calculations employed the experimental structure (ref.[18], cf. Figure 1a) and the "full basis" (i.e. IGLO-II bases on all ligand atoms). Experimental ^{13}C shift tensors from ref.[2]. ^{13}C shifts vs. TMS, ^{17}O shifts vs. H_2O^{vap}. – [b] Shift anisotropy $(\delta_{11} + \delta_{22})/2 - \delta_{33}$.

The dependence of the bridging carbonyl ^{13}C shift tensor on the asymmetry of the bridge is probed in Table 2. Note the good agreement between the results given for the experimental structure A_0 and those in Table 1. Obviously, the mixed-basis approximation used for the data in Table 2 is very well justified. Upon going from the symmetrically bridged experimental structure A_0 to the extremely unsymmetrical bridge in structure A_3, δ_{33} decreases considerably. This leads to a simultaneous decrease in δ_{av} and to an increased shift anisotropy. These results closely parallel those obtained by Hawkes et al.[2] when comparing MAS spectra for semi-bridging CO ligands in different iron carbonyl clusters. The main difference in our computational study is the presence of an identical set of auxiliary terminal ligands for all four structures A_0–A_3. Thus, we have separated the structural contributions from the influence of the remaining substituents. The LMO breakdown indicates that changes in the deshielding contributions from bridging LMOs account for the changes in δ_{33}.

Table 2. Dependence of bridging CO chemical shift tensors (ppm) in $Fe_2(CO)_9$ on bridging character[a]

structure	δ_{11}	δ_{22}	δ_{33}	δ_{av}	$\Delta\delta^c$
C_{bridge}					
//exp. $(A_0)^b$	313.	269.	194.	259.	97.
$//A_1{}^b$	311.	269.	184.	255.	106.
$//A_2{}^b$	323.	260.	144.	242.	147.
$//A_3{}^b$	335.	311.	12.	219.	311.

[a] ^{13}C shifts vs. TMS. Mixed ECP/basis approach (cf. computational details section). – [b] Cf. Figure 1 for the structures A_0–A_3. – [c] Shift anisotropy $(\delta_{11} + \delta_{22})/2 - \delta_{33}$.

B. Chemical Shift Tensors in $Rh_6(CO)_{16}$

Table 3 gives the calculated shift tensors for both bridging and terminal carbonyl ligand nuclei in $Rh_6(CO)_{16}$ (see structure in Figure 2). Experimetal ^{13}C data are also included whereas the oxygen shift tensors have not been measured up to now. Agreement between computed and experimental ^{13}C shift tensors is excellent, particularly so for the bridging ligands. Due to the presence of a threefold rotational axis through the bridging CO ligand and the bridged Rh_3 face, the bridging ligand shift tensors have axial symmetry (the shift tensors of the terminal ligands deviate slightly from axial symmetry). The calculations clearly confirm the very large δ_{33} for the bridging carbon and thus the very small shift anisotropy. On the other hand, the terminal carbon chemical shift tensor is unremarkable. Interestingly, the bridge oxygen atoms also exhibit very large δ_{33}, an extremely small anisotropy, and also a large δ_{av}. This is a computational prediction for which experimental confirmation would be desirable. The larger δ_{11} and δ_{22} compared to the terminal oxygen nuclei are notable, as they contrast to the situation for the carbon shifts. However, this behavior is consistent with the above results for $Fe_2(CO)_9$. The computed terminal carbonyl oxygen shift tensor compares well to other typical examples[10,29].

An LMO analysis of the shielding tensors is more fruitful than for $Fe_2(CO)_9$. The localization procedure gives the expected C≡O bonds, oxygen lone pairs, and terminal Rh–CO bonds (and the carbon and oxygen 1s orbitals). Additionally, it finds four nonbonding d orbitals [plus an $(n - 1)sp^3$-set] for each metal, three "metal-metal bonding" LMOs, and four four-center CRh_3 LMOs (essentially lone-pairs on the bridging carbon atoms pointing towards the center of the bridged triangle of the Rh_6 octahedron). As the three M–M bonding LMOs (which do not match the molecular symmetry) do not contribute much to the ligand shielding tensors, the analysis is reasonably straightforward. The results of the LMO breakdown of a bridging carbon shielding tensor are summarized in Table 4, those for a terminal carbonyl ligand in Table 5.

The four-center CRh_3 bonding orbital mentioned above gives contributons to the bridging ^{13}C shielding tensor

Table 3. Chemical shift tensors (ppm) for $Rh_6(CO)_{16}$[a]

		δ_{11}	δ_{22}	δ_{33}	δ_{av}	$\Delta\delta^b$
C_{bridge}	calc.	293.	293.	106.	231.	187.
	exp.[c]	296.	296.	102.	231.	194.
	exp.[d]	301.	292.	97.	230.	199.
C_{termnl}	calc.	335.	312.	-81.	189.	405.
	exp.[c]	315.	305.	-80.	180.	390.
	exp.[d]	320.	299.	-76.	181.	386.
O_{bridge}	calc.	626.	626.	574.	609.	51.
O_{termnl}	calc.	591.	522.	-25.	363.	582.

[a] The calculations employed the experimental structure (ref.[22], see Figure 2). ^{13}C shifts vs. TMS, ^{17}O shifts vs. H_2O^{vap}. – [b] Shift anisotropy $(\delta_{11} + \delta_{22})/2 - \delta_{33}$. – [c] Broad-line static results from ref.[1]. – [d] Slow-spinning MAS results from ref.[3a].

Table 4. LMO Breakdown of $\sigma(^{13}CO_{bridge})$ in $Rh_6(CO)_{16}$[a]

LMO	$\sigma_\perp$	$\sigma_\parallel$	σ_{av}	$\Delta\sigma^b$
1s(C)	200.0	200.0	200.0	
LP(O)	-50.1	+3.4	-32.3	
3xBd(C≡O)	-68.5	+126.3	-3.3	
LP(C)/Bd(C-$(Rh)_3$)[c]	-184.0	26.9	-115.7	
Σwithout AO(M)[d]	-102.2	+356.6	+48.7	-458.8
ΣAO($Rh_{1,2,3}$)[e]	-5.8	-73.7	-27.8	
Σ[f]	-119.7	+135.4	-34.8	-255.1
Total:[g]	-105.8	+81.5	-43.3	-187.3

[a] Absolute shieldings in ppm. Only LMOs with at least one individual contribution >3 ppm were included. Our notation is: LP = lone pair, Bd = bond. – [b] Shielding anisotropy $(\sigma_{11} + \sigma_{22})/2 - \sigma_{33}$. – [c] LMO pointing from the bridging carbon atom towards the center of the bridged metal triangle. – [d] Metal AO contributions excluded. – [e] Sums of contributions from metal $(n - 1)$p-AO (semicore) and $(n - 1)$d-AO-like LMOs, centered on the three bridged metal centers. – [f] Sum of all listed contributions. – [g] Sum of all contributions.

(Table 4) which are very similar to those of the C–M σ bonding LMOs for terminal carbonyl ligands (Table 5), namely large deshielding contributions to $\sigma_\perp$ but small shielding contributions to $\sigma_\parallel$. The much smaller shift anisotropy (and larger shift) for the bridging ligand is not caused by this orbital but by significant deshielding contributions to σ_{33} ($\sigma_\parallel$) from nonbonding $(n - 1)$p- and d orbital-like

Table 5. LMO Breakdown of $\sigma(^{13}CO_{termnl})$ in $Rh_6(CO)_{16}$[a]

LMO	σ_{11}	σ_{22}	σ_{33}	σ_{av}
1s(C)	200.0	200.0	200.0	200.0
LP(O)	-52.6	-50.2	3.4	-33.1
3xBd(C≡O)	-87.8	-91.9	52.5	-42.4
Bd(C-Rh)[b]	-181.8	-159.4	22.4	-106.3
Σwithout AO(M)[c]	-122.2	-101.5	278.3	18.2
ΣAO(Rh)[d]	-31.2	-31.0	-14.4	-25.6
Σ[e]	-153.4	-132.5	263.9	-7.4
Total:[f]	-147.6	-124.3	267.8	-1.4

[a] Absolute shieldings in ppm. Only LMOs with at least one individual contribution >3 ppm were included. Our notation is: LP = lone pair, Bd = bond. – [b] C–M σ-bonding LMO. – [c] Metal AO contributions excluded. – [d] Sums of contributions from metal (n – 1)p-AO (semicore) and (n – 1)d-AO-like LMOs, centered on the neighboring metal center. – [e] Sum of all listed contributions. – [f] Sum of all contributions.

LMOs on the three metal centers that are bridged by this ligand [summarized under $\Sigma AO(Rh_{1,2,3})$ in Table 4]. Thus, the LMO analysis gives results which are very similar to those obtained for the terminal carbonyl shielding tensors in the unusual, highly reduced group-4 piano-stool and bent-sandwich carbonyl complexes $[MCp(CO)_4^-$, $MCp_2(CO)_2$; M = Ti, Zr, Hf] of ref.[9]. Formally nonbonding metal d orbitals also accounted for the deshielded σ_{33} in these cases.

C. ELF Plots

The ambiguity of orbital localization procedures in delocalized, highly symmetrical clusters like $Fe_2(CO)_9$ and $Rh_6(CO)_{16}$ makes a consistent localized MO description of the bonding difficult. A more rigorous localized view may be provided by quantities like the Laplacian of the charge density[30] or by the electron localization function (ELF)[13]. The ELF has been shown to give appreciable insight into bonding in molecules, clusters, and solids[13,31]. It is unique also for systems with high symmetry and multi-center bonding. ELF is close to 1 in regions of covalent bonds, lone pairs or core shells, close to 0 in regions "between shells"[13].

The graphical representation chosen here is that of iso-ELF surfaces. Figure 3 shows an isosurface (ELF = 0.7) for $Fe_2(CO)_9$. An ELF isosurface of this value is an envelope encompassing regions of high electron localization. For the bridging carbonyls, the plot clearly indicates less localization in the C≡O bonding region but a more extended oxygen lone-pair region compared to the terminal ligands. This agrees with the notion of considerable backbonding into π*-CO orbitals in the bridging position[32]. The plot also shows the absence of axial symmetry for the bridging CO ligand. No direct metal-metal covalent bonding is indicated by the ELF. The localization of the Fe–C–Fe bridging electrons is close to the bridging carbon atoms. This bonding picture is consistent with previous MO studies[33] and also with a recent plot of the Laplacian of the charge density[32]. The metal valence localization region is characterized by an almost cube-shaped distribution. We find this to be a typical feature of octahedrally coordinated transition metals. More generally, the nonbonding valence localization region tends to be arranged in form of a dual polyhedron with respect to the ligand polyhedron[34].

Figure 3. Isosurface ELF = 0.7 for $Fe_2(CO)_9$ together with a ball-and-stick model of the molecular structure. An ELF isosurface of this value is an envelope encompassing regions of high electron localization, as may typically be associated with core shells, bonds, or lone pairs

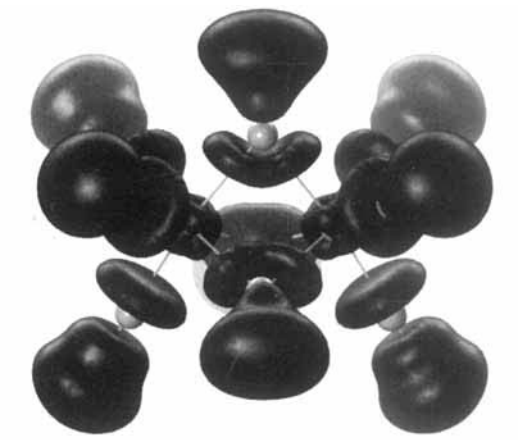

A view of an ELF = 0.7 isosurface for $Rh_6(CO)_{16}$ from the inside of the Rh_6 octahedron through a Rh_3 face on the bridging carbonyl ligand is given in Figure 4. One can clearly distinguish the nearly cube-shaped nonbonding metal valence distributions and the carbon "lone-pair" (CRh3 4-center bond) directed towards the center of the face and deviating only little from axial symmetry. The differences between terminal and bridging CO ligands are seen clearly when comparing side-on views (Figure 5). Again, the C≡O bonding high-ELF region of the bridging ligand is depleted, and the oxygen lone-pair region is extended compared to the terminal ligand, consistent with extensive back-bonding for the former (cf. above). The "carbon lone-pair" (C–M bonding region) of the bridging ligand is more curved and contracted than that of the terminal ligand.

We have looked for an indication of electron localization representing metal–metal bonding within the cluster. Indeed, maxima peaking at ca. ELF = 0.62 are found slightly above the centers of those four faces of the Rh_6 octahedron which are not occupied by bridging carbonyl ligands. It is known that bonds involving transition metals and d orbitals lead to relatively low localization maxima in the ELF representation, due to the occurrence of the angular momentum quantum numbers in the denominator of the ELF expression[35]. An isosurface view of these ELF domains is given in Figure 6. Taking into account the usual electron count[36] for this closo cluster, these four ELF maxima

Figure 4. Isosurface ELF = 0.7 for $Rh_6(CO)_{16}$. View from the inside of the Rh_6 octahedron through a bridged face on top of the bridging carbonyl carbon atom. At the sides, remainders of ELF distributions from terminal ligands are seen

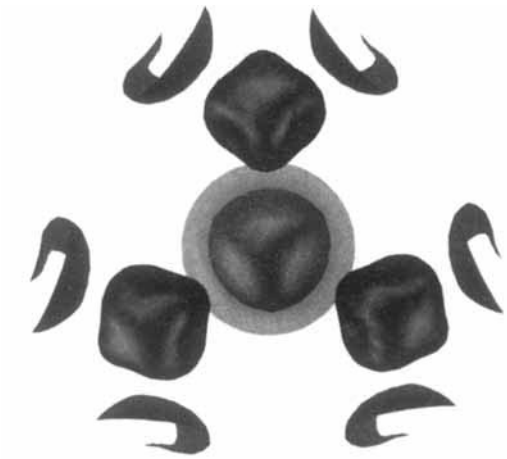

Figure 5. Side views of ELF = 0.7 isosurfaces for CO groups in $Rh_6(CO)_{16}$. A Terminal ligand, B bridging ligand

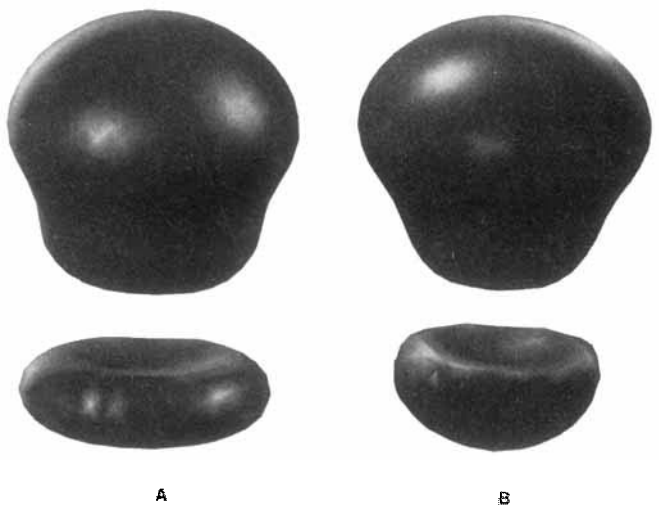

correspond to six bonding electrons. Thus, one may assign 3/2 electrons to each of the unbridged faces of the octahedron. The other four faces are "held together" by the bridging carbonyl ligands. No ELF maximum is found at the center of the cluster. Probably, this is as close as one can get to a localized description of bonding within the Rh_6 unit. ELF maxima above the polyhedral faces are also characteristic for boron clusters[31a]. For example, for $B_6H_6^{2-}$, the cluster-bonding ELF-maxima cap all of the octahedral faces, and a cuboidal arrangement is found[31a]. In analogy, the four bridging carbonyl carbon "lone-pairs" together with the four additional ELF maxima above the unbridged faces (Figure 6) may be viewed as a heterocubane-type arrangement of the cluster-bonding ELF domains.

Figure 6. Isosurface ELF = 0.45 for $Rh_6(CO)_{16}$. Viewpoint as in Figure 4. Note four maxima at the centers of the four unbridged octahedral faces. These may be associated with the 3-center-3/2-electron bonds discussed in the text. The isosurface is cut open by the limits of the cube of calculation points

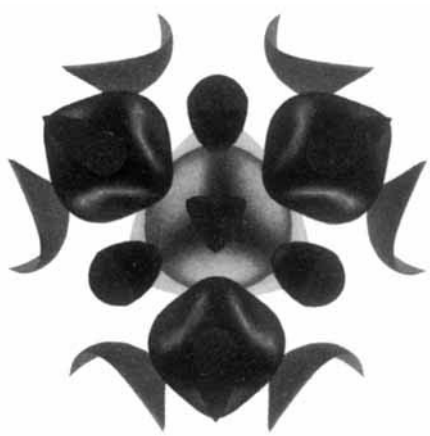

4. Conclusions

Ligand NMR chemical shift tensors in systems as complex as the multinuclear transition-metal clusters studied here are now accessible to detailed quantitative computation due to the relatively low computational effort and remarkably high accuracy of approaches based on density-functional theory. This allows the further analysis of the ligand chemical shielding mechanisms in transition-metal compounds because, for example the computations yield the principal axes of the tensors that are not easily available from experiment. Moreover, the calculations were also used to predict ^{17}O shift tensors. We hope this will stimulate further experimental work.

The breakdown of the shielding tensors into contributions from localized molecular orbitals becomes less useful for larger, more delocalized systems. Nevertheless, our calculations indicate that metal-centered nonbonding orbitals account for the large δ_{33} and for the low shift anisotropy values (both ^{13}C and ^{17}O) of the bridging carbonyl group in $Rh_6(CO)_{16}$. This resembles the situation for the unusual four-legged piano-stool d^4 and bent-sandwich d^2 carbonyl complexes of Ti, Zr, and Hf, which we studied previously[9]. Obviously, the presence of nonbonding metal orbitals in a favorable spatial arrangement has a significant influence on carbonyl chemical shift tensors.

Electron localization functions (ELF) give a useful graphical representation of differences in the electronic structure between bridging and terminal ligands. Interestingly, ELF indicates that the cluster-bonding electrons in $Rh_6(CO)_{16}$ are mainly localized on the four unbridged faces of the Rh_6 octahedron, giving rise to four "3-center-3/2-electron bonds". The resulting "heterocubane-like" distribution of ELF maxima above all octahedral faces fits nicely with previous results on boron cluster compounds[31a].

I am grateful to Dr. *V. G. Malkin* and *O. Malkina* (Bratislava) as well as to Dr. *U. Wedig* (Stuttgart) for helpful discussions. I also thank the *Deutsche Forschungsgemeinschaft* (Germany) for a "Habilitationsstipendium" and Prof. *H. G. von Schnering* (Max-Planck-

Institut, Stuttgart) and Prof. *H.-J. Werner* (Universität Stuttgart) for their support and for providing computational resources.

---

* Dedicated to Professor *Hans Georg von Schnering* on the occasion of his 65th birthday.

[1] J. W. Gleeson, R. W. Vaughan, *J. Chem. Phys.* **1983**, *78*, 5384.

[2] G. E. Hawkes, K. D. Sales, S. Aime, R. Gobetto, L.-Y. Lian, *Inorg. Chem.* **1991**, *30*, 1489.

[3] [3a] T. H. Walter, L. Reven, E. Oldfield, *J. Phys. Chem.* **1989**, *93*, 1320. – [3b] S. Aime, M. Botta, R. Gobetter, D. Osella, L. Milone, *Inorg. Chim. Acta* **1988**, *146*, 151. – [3c] H. W. Spiess, R. Grosescu, U. Haeberlen, *Chem. Phys.* **1974**, *6*, 226.

[4] H. C. Dorn, B. E. Hanson, E. Motell, *J. Organomet. Chem.* **1982**, *224*, 181.

[5] See, e.g.: J. E. Ellis, S. R. Frerichs, B. Kelsey Stein, *Organometallics* **1993**, *12*, 1048; cf. ref.[9] for a more extensive bibliography.

[6] [6a] V. G. Malkin, O. L. Malkina, M. E. Casida, D. R. Salahub, *J. Am. Chem. Soc.* **1994**, *116*, 5898. – [6b] V. G. Malkin, O. L. Malkina, L. A. Eriksson, D. R. Salahub in *Theoretical and Computational Chemistry*, vol. 2 (Eds.: P. Politzer, J. M. Seminario), Elsevier, Amsterdam, **1995**.

[7] M. Kaupp, V. G. Malkin, O. L. Malkina, D. R. Salahub, *Chem. Phys. Lett.* **1995**, *235*, 382.

[8] M. Kaupp, V. G. Malkin, O. L. Malkina, D. R. Salahub, *J. Am. Chem. Soc.* **1995**, *117*, 1851.

[9] M. Kaupp, *Chem. Eur. J.* **1996**, *2*, 194.

[10] M. Kaupp, V. G. Malkin, O. L. Malkina, D. R. Salahub, *Chem. Eur. J.* **1996**, *2*, 24.

[11] Apart from the present work, good results with multinuclear clusters have also been obtained for ^{13}C shift tensors of interstitial carbides in carbonyl clusters (M. Kaupp, submitted).

[12] J. P. Hickey, J. R. Wilkinson, L. J. Todd, *J. Organomet. Chem.* **1979**, *179*, 159; S. Aime, D. Osella, L. Milone, G. E. Hawkes, E. W. Randall, *J. Am. Chem. Soc.* **1981**, *103*, 5920.

[13] A. D. Becke, K. E. Edgecombe, *J. Chem. Phys.* **1990**, *92*, 5397; A. Savin, A. D. Becke, J. Flad, R. Nesper, H. G. von Schnering, *Angew. Chem.* **1991**, *103*, 421; *Angew. Chem. Int. Ed. Engl.* **1991**, *30*, 409.

[14] W. Kutzelnigg, U. Fleischer, M. Schindler in *NMR-Basic Principles and Progress*, Springer Verlag, Heidelberg, **1990**, vol. 23, p. 165.

[15] J. M. Foster, S. F. Boys, *Rev. Mod. Phys.* **1963**, *35*, 457.

[16] J. P. Perdew, Y. Wang, *Phys. Rev. B* **1992**, *45*, 13244; J. P. Perdew in *Electronic Structure of Solids* (Eds.: P. Ziesche, H. Eischrig), Akademie Verlag, Berlin, **1991**; J. P. Perdew, J. A. Chevary, S. H. Vosko, K. A. Jackson, M. R. Pederson, D. J. Singh, C. Fiolhais, *Phys. Rev. B* **1992**, *46*, 6671.

[17] D. R. Salahub, R. Fournier, P. Mlynarski, I. Papai, A. St-Amant, J. Ushio in *Density Functional Methods in Chemistry* (Eds.: J. K. Labanowski, J. W. Andzelm), Springer, New York, **1991**, p. 77; A. St-Amant, D. R. Salahub, *Chem. Phys. Lett.* **1990**, *169*, 387; A. St-Amant, Thesis, Université de Montréal, **1992**.

[18] F. A. Cotton, J. M. Troup, *J. Chem. Soc., Dalton Trans.* **1974**, 800.

[19] F. A. Cotton, J. M. Troup, *J. Am. Chem. Soc.* **1974**, *96*, 4155.

[20] D. J. Dahm, R. A. Jacobson, *J. Am. Chem.Soc.* **1968**, *90*, 5106.

[21] Y. Degreve, J. Meunier-Piret, M. Van Meersche, P. Piret, *Acta Crystallogr.* **1967**, *23*, 119.

[22] E. R. Corey, L. F. Dahl, W. Beck, *J. Am. Chem. Soc.* **1963**, *85*, 1202.

[23] M. Dolg, U. Wedig, H. Stoll, H. Preuss, *J. Chem. Phys.* **1987**, *86*, 866.

[24] D. Andrae, U. Häußermann, M. Dolg, H. Stoll, H. Preuss, *Theor. Chim. Acta* **1990**, *77*, 123.

[25] A. Bergner, M. Dolg, W. Küchle, H. Stoll, H. Preuss, *Mol. Phys.* **1993**, *80*, 1431.

[26] D. B. Chesnut, K. D. Moore, *J. Comp. Chem.* **1989**, *10*, 648.

[27] N. Godbout, D. R. Salahub, J. Andzelm, E. Wimmer, *Can. J. Chem.* **1992**, *70*, 560.

[28] Program *TURBOMOLE*, Universität Karlsruhe, version **1989**; M. Häser, R. Ahlrichs, *J. Comp. Chem.* **1988**, *10*, 104.

[29] E. Oldfield, M. A. Keniry, S. Shinoda, S. Schramm, T. L. Brown, H. S. Gutowsky, *J. Chem. Soc., Chem. Commun.* **1985**, 791.

[30] R. W. F. Bader, *Atoms in Molecules. A Quantum Theory*, Clarendon Press, Oxford, UK, **1990**.

[31] [31a] A. Burkhardt, U. Wedig, H. G. von Schnering, A. Savin, *Z. Anorg. Allg. Chem.* **1993**, *619*, 437. – [31b] A. Savin, O. Jepsen, J. Flad, O. K. Andersen, H. Preuss, H. G. von Schnering, *Angew. Chem.* **1992**, *104*, 186; *Angew. Chem. Int. Ed. Engl.* **1992**, *31*, 187. – [31c] U. Häussermann, S. Wengert, P. Hofmann, A. Savin, O. Jepsen, R. Nesper, *Angew. Chem.* **1994**, *106*, 2147; *Angew. Chem. Int. Ed. Engl.* **1994**, *33*, 2069. – [31d] U. Häussermann, S. Wengert, R. Nesper, *Angew. Chem.* **1994**, *106*, 2150; *Angew. Chem. Int. Ed. Engl.* **1994**, *33*, 2073. – [31e] H. G. von Schnering, R. H. Cardoso Gil, W. Hönle, A. Burkhardt, G. Krier, O. K. Andersen, *Angew. Chem.* **1995**, *107*, 81; *Angew. Chem. Int. Ed. Engl.* **1995**, *34*, 103. – [31f] Y. Grin, U. Wedig, H. G. von Schnering, *Angew. Chem.* **1995**, *107*, 1318; *Angew. Chem. Int. Ed. Engl.* **1995**, *34*, 1204.

[32] C. Bo, J.-P. Sarasa, J.-M. Poblet, *J. Phys. Chem.* **1993**, *97*, 6362.

[33] R. H. Summerville, R. Hoffmann, *J. Am. Chem. Soc.* **1979**, *101*, 3821; C. W. Bauschlicher, Jr., *J. Chem. Phys.* **1986**, *84*, 872.

[34] M. Kaupp, unpublished results. A similar dual behavior also holds for the relation between nuclear positions and ELF distributions in boron clusters (cf. ref.[31a]) and in intermetallic phases (Y. Grin, personal communication).

[35] M. Kohout, A. Savin, to be published (M. Kohout, personal communication).

[36] F. A. Cotton, G. Wilkinson, *Advanced Inorganic Chemistry*, Wiley Interscience, 5th Ed., New York, **1988**.

[95218]